Progress of Theoretical Physics, Vol. 121, No. 4, April 2009

Strange Nonchaotic Responses of the Quasiperiodically Forced Morris-Lecar Neuron

Woochang LIM,[1,*] Sang-Yoon KIM[1,2,**] and Youngtae KIM[3,***]

[1]*Department of Physics, Kangwon National University, Chunchon, Kangwon-Do 200-701, Korea*
[2]*Department of Physics, University of Wisconsin-Milwaukee, P.O. Box 413, Wisconsin 53211, USA*
[3]*Department of Physics, Ajou University, Suwon 442-749, Korea*

(Received November 14, 2008)

We study dynamical responses of the self-oscillating Morris-Lecar (ML) neuron under quasiperiodic stimulation. For the case of periodic stimulation on the self-oscillating ML neuron, a transition from a periodic to a chaotic oscillation occurs through period doublings. We investigate the effect of the quasiperiodic forcing on this period-doubling route to chaotic oscillation. In contrast to the periodically-forced case, a new type of strange nonchaotic (SN) oscillating states (that are geometrically strange but have no positive Lyapunov exponents) is thus found to appear between the regular and chaotic oscillating states. Strange fractal geometry of these SN oscillating states, which is characterized in terms of the phase sensitivity exponent and the distribution of local finite-time Lyapunov exponent, leads to aperiodic "complex" spikings. Diverse routes to SN oscillations are found, as in the quasiperiodically forced logistic map.

Subject Index: 034, 552

§1. Introduction

To probe dynamical properties of a system, one often applies an external stimulation to the system and study its dynamical response. Particularly, much attention has been paid to various periodically stimulated biological systems such as the embryonic chick heart-cell aggregates[1)] and the squid giant axon.[2)] These periodically forced systems have been found to exhibit rich regular and chaotic behaviors.[3)] In contrast to the (well-understood) periodically forced case, quasiperiodically forced case has received little attention.[4)] Hence, intensive investigation of quasiperiodically forced biological oscillators is necessary for understanding their dynamical responses under the quasiperiodic forcing.

Strange nonchaotic (SN) states typically appear between the regular and chaotic states in quasiperiodically forced dynamical systems.[5)–16)] These SN attractors show some properties of regular as well as chaotic attractors. Like regular attractors, they exhibit nonchaotic dynamics in the sense that they do not have a positive Lyapunov exponent; like usual chaotic attractors, they have a geometrically strange fractal structure. Here, we are interested in dynamical responses of quasiperiodically

*) E-mail: wclim@kangwon.ac.kr
**) Corresponding author. E-mail:sykim@kangwon.ac.kr
***) E-mail: ytkim@ajou.ac.kr

stimulated neurons and SN responses are expected to occur.

This paper is organized as follows. In §2, we study dynamical responses of the quasiperiodically-forced self-oscillating Morris-Lecar (ML) neuron.[17)–19)] The effect of periodic forcing on the self-oscillating neurons was previously studied, and regular and chaotic responses were found.[2),20)] However, to the best of our knowledge, so far there are no works on the quasiperiodically forced neurons. Here, we study the case of quasiperiodic stimulation with two incommensurate frequencies, and compare the dynamical responses with those for the case of periodic stimulus. In the periodically forced case (i.e., in the presence of only one ac stimulus source), a transition from a periodic to a chaotic oscillation is found to occur via an infinite sequence of period-doubling bifurcations.[21)] We investigate the effect of the quasiperiodic forcing on this period-doubling route to chaotic oscillation by adding another independent ac stimulus source. Thus, in contrast to the case of periodic forcing, a new type of SN oscillating states is found to appear between the regular and chaotic oscillating states. We characterize the strangeness of SN attractors in terms of the phase sensitivity exponent and the distribution of local finite-time Lyapunov exponent.[10)] Due to their strange geometry, SN oscillating states give rise to the appearance of aperiodic complex spikings. Diverse dynamical routes to SN oscillating states are identified, as in the quasiperiodically forced logistic map. Finally, a summary is given in § 3.

§2. SN oscillations in the quasiperiodically forced ML neuron

We consider the conductance-based ML neuron model, originally proposed to describe the time-evolution pattern of the membrane potential for the giant muscle fibers of barnacles.[17)–19)] The dynamics of the ML neuron, which is quasiperiodically forced at two incommensurate frequencies f_1 and f_2, is governed by the following set of differential equations:

$$\begin{aligned} C\frac{dV}{dt} &= -I_{ion} + I_{ext} = -(I_{Ca} + I_K + I_L) + I_{ext} \\ &= -g_{Ca} m_\infty(V)(V - V_{Ca}) - g_K w(V - V_K) - g_L(V - V_L) + I_{ext}, \quad (2\cdot1a) \\ \frac{dw}{dt} &= \phi \frac{(w_\infty(V) - w)}{\tau_R(V)}, \quad (2\cdot1b) \end{aligned}$$

where

$$m_\infty(V) = 0.5\,[1 + \tanh\{(V - V_1)/V_2\}]\,, \quad (2\cdot2a)$$

$$w_\infty(V) = 0.5\,[1 + \tanh\{(V - V_3)/V_4\}]\,, \quad (2\cdot2b)$$

$$\tau_R(V) = 1/\cosh\{(V - V_3)/(2V_4)\}\,. \quad (2\cdot2c)$$

Here, the external stimulus current density (measured in units of μA/cm^2) is given by $I_{ext} = I_{dc} + A_1 \sin(2\pi f_1 t) + A_2 \sin(2\pi f_2 t)$, I_{dc} is a dc stimulus, A_1 and A_2 are amplitudes of quasiperiodic forcing, and $\omega(\equiv f_2/f_1)$ is irrational (f_1 and f_2: measured in units of kHz). The state of the ML neuron at a time t (measured in units of ms) is characterized by two state variables: the membrane potential V (measured in units of mV) and the slow recovery variable w representing the activation

of the K^+ current (i.e., the fraction of open K^+ channels). In Eq. (2·1a), C denotes the capacitance of the membrane, and the total ionic current consists of the calcium current I_{Ca}, the potassium current I_K, and the leakage current I_L. Each ionic current obeys Ohm's law. The constants g_{Ca}, g_K, and g_L are the maximum conductances for the ion and leakage channels, and the constants V_{Ca}, V_K, and V_L are the corresponding equilibrium potentials at which each current is balanced by the ionic concentration difference across the membrane. Since the calcium current I_{Ca} changes much faster than the potassium current I_K, the gate variable m for the Ca^{2+} channel is assumed to always take its saturation value m_∞. On the other hand, the activation variable w for the K^+ channel approaches its saturation value w_∞ with the relaxation time $\tau_R(V)/\phi$, where τ_R has a dimension of ms and ϕ is a (dimensionless) temperaturelike time scale factor. The ML neuron may be either type-I or type-II depending on the system parameters.[18] For the case of a type-I (type-II) neuron, the firing frequency begins to increase from zero (a nonzero finite value) when I_{dc} passes a threshold value. Here, we consider the case of type-II excitability where $g_{Ca} = 4.4$ mS/cm^2, $g_K = 8$ mS/cm^2, $g_L = 2$ mS/cm^2, $V_{Ca} = 120$ mV, $V_K = -84$ mV, $V_L = -60$ mV, $C = 20$ μF/cm^2, $\phi = 0.04$, $V_1 = -1.2$ mV, $V_2 = 18$ mV, $V_3 = 2$ mV, and $V_4 = 30$ mV.[18]

For getting the Poincaré map of Eq. (2·1), we make a normalization $f_1 t \to t$, and then Eq. (2·1) can be reduced to the following differential equations:

$$\begin{aligned}\frac{dV}{dt} &= F_1(\boldsymbol{x},\theta)\\ &= \frac{1}{C\ f_1}[-g_{Ca}m_\infty(V)(V-V_{Ca}) - g_K w(V-V_K)\\ &\quad -g_L(V-V_L)+I_{ext}], \qquad (2\cdot3a)\\ \frac{dw}{dt} &= F_2(\boldsymbol{x},\theta) = \frac{\phi}{f_1}\frac{(w_\infty(V)-w)}{\tau_R(V)}, \qquad (2\cdot3b)\\ \frac{d\theta}{dt} &= \omega, \quad (\mathrm{mod}\ 1) \qquad (2\cdot3c)\end{aligned}$$

where $\boldsymbol{x}[=(x_1,x_2)] \equiv (V,w)$ and $I_{ext} = I_{dc} + A_1\sin(2\pi t) + A_2\sin(2\pi\theta)$. The phase space of the quasiperiodically forced ML oscillator is four dimensional with coordinates V, w, θ, and t. Since the system is periodic in θ and t, they are circular coordinates in the phase space. Then, we consider the surface of section, the V-w-θ hypersurface at $t = n$ (n: integer). The phase-space trajectory intersects the surface of section in a sequence of points. This sequence of points corresponds to a mapping on the three-dimensional hypersurface. The map can be computed by stroboscopically sampling the orbit points $\boldsymbol{v}_n$ $[\equiv (\boldsymbol{x}_n,\theta_n)]$ at the discrete time n (corresponding to multiples of the first external driving period T_1). We call the transformation $\boldsymbol{v}_n \to \boldsymbol{v}_{n+1}$ the Poincaré map, and write $\boldsymbol{v}_{n+1} = P(\boldsymbol{v}_n)$.

Equations (2·1) and (2·3c) are numerically integrated by using the fourth-order Runge-Kutta method. Dynamical analysis is done in both the continuous-time system (i.e., flow) and the discrete-time system (i.e., Poincaré map). For example, the time series of the membrane potential $V(t)$ and the phase flow are obtained in the flow. On the other hand, the Lyapunov exponent[22] and the phase

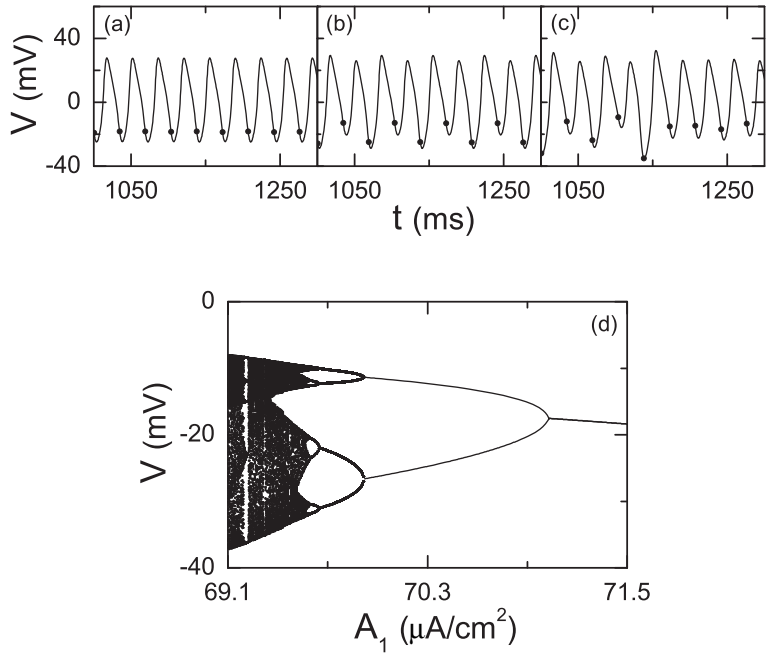

Fig. 1. Period-doubling transition to chaos in the periodically forced ML oscillator for $I_{dc} = 200$ μA/cm^2 and $f_1 = 29$ Hz ($A_2 = 0$). Time series of $V(t)$ for (a) $A_1 = 71.2$ μA/cm^2, (b) $A_1 = 70.3$ μA/cm^2, and (c) $A_1 = 69.3$ μA/cm^2, which correspond to the period-1, period-2, and chaotic states in the Poincaré map P (solid circles represent stroboscopically sampled points in P), respectively. The largest Lyapunov exponent for the chaotic oscillation in (c) is $\sigma_1 \simeq 0.334$. (d) Bifurcation diagram (i.e., plot of V versus A_1) in P.

sensitivity exponent[10] are calculated in the Poincaré map P. To get the Lyapunov exponent of an attractor in the Poincaré map, we choose 20 random initial points $\{(V_i(0), w_i(0), \theta_i(0)); i = 1, \ldots, 20\}$ with uniform probability in the range of $V_i(0) \in (-20, 20)$, $w_i(0) \in (0.4, 0.5)$, and $\theta_i(0) \in [0, 1)$. For each initial point, we obtain the Lyapunov exponent, and choose the average value of the 20 Lyapunov exponents. (The method of getting the phase sensitivity exponent will be given below.)

In the presence of only the dc stimulus (i.e., $A_1 = A_2 = 0$), a transition from a silent state to a periodic spiking state occurs for $I_{dc} = I_{dc}^*$ ($\simeq 93.9$ μA/cm^2) through a subcritical Hopf bifurcation as the silent state absorbs the unstable limit cycle born via a fold limit cycle bifurcation for $I_{dc} \simeq 88.3$ μA/cm^2.[18] Thus, a self-sustained oscillation (corresponding to a spiking state) is induced in the ML neuron for $I_{dc} > I_{dc}^*$. Here, we set $I_{dc} = 200$ μA/cm^2 and ω to be the reciprocal of the golden mean [i.e., $\omega = (\sqrt{5} - 1)/2$], and numerically investigate dynamical responses of the self-oscillating ML oscillator under the ac external stimulus. We first study the periodically-forced case (i.e., $A_2 = 0$) by changing A_1 for $f_1 = 29$ Hz. The time

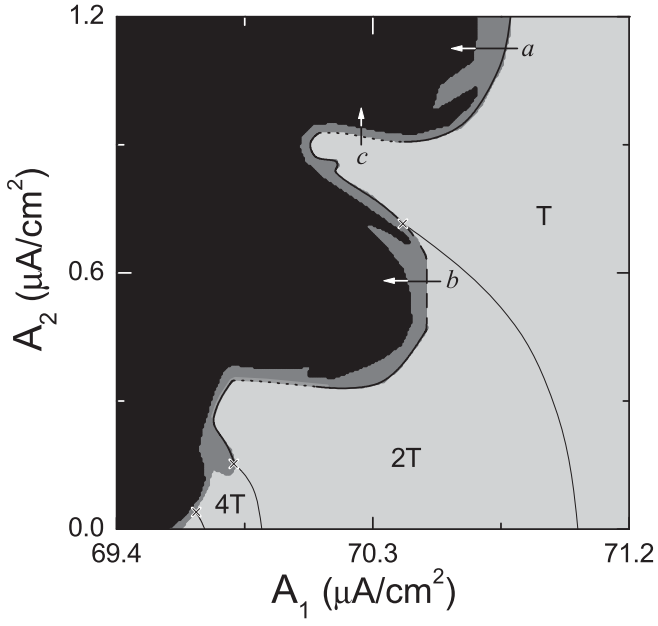

Fig. 2. State diagram in the A_1-A_2 plane for $I_{dc} = 200$ μA/cm^2 and $f_1 = 29$ Hz in the quasiperiodically forced ML oscillator. Regular, SN, and chaotic regions are shown in light gray, gray, and black, respectively. In the regular region, the torus, the doubled torus, and the quadrupled torus exist in the regions denoted by T, $2T$, and $4T$, respectively, and the solid lines represent torus doubling bifurcation curves with terminal points denoted by crosses. SN attractors appear via various routes when passing the heavy solid line, the dashed line, and the dotted line.

series of $V(t)$ for $A_1 = 71.2$, 70.3, and 69.3 μA/cm^2 are shown in Figs. 1(a)–(c), respectively, and the bifurcation diagram in the Poincaré map P is also given in Fig. 1(d); stroboscopically sampled points in P are represented by solid circles in Figs. 1(a)–(c). Successive period-doubling bifurcations occur as A_1 is decreased. For example, periodic oscillations of $V(t)$ in Figs. 1(a) and 1(b) correspond to period-1 and period-2 states in P, respectively. As A_1 passes a threshold A_1^* (= 69.576 779 μA/cm^2) a chaotic transition occurs. Thus, for $A_1 < A_1^*$ chaotic oscillations with positive Lyapunov exponents appear [e.g., see Fig. 1(c)].

We now investigate the effect of quasiperiodic forcing on the period-doubling route to chaotic oscillation by varying A_1 and A_2 for $f_1 = 29$ Hz. A state diagram in the A_1-A_2 plane is shown in Fig. 2. We characterize each state in terms of the largest (nontrivial) Lyapunov exponent σ_1, associated with dynamics of the variable $\boldsymbol{x}$ [besides the (trivial) zero exponent, related to the phase variable θ of the quasiperiodic forcing] and the phase sensitivity exponent δ. The exponent δ measures the sensitivity of the variable $\boldsymbol{x}$ with respect to the phase θ of the quasiperiodic forcing and characterizes the strangeness of an attractor.[10] A smooth torus that has a negative largest Lyapunov exponent (i.e., $\sigma_1 < 0$) without phase sensitivity

(i.e., $\delta = 0$) exists in the region denoted by T and shown in light gray. Regular quasiperiodic oscillations occur on these smooth tori. When crossing a solid line, the smooth torus becomes unstable and bifurcates to a smooth doubled torus in the region represented by $2T$. These doubled tori also bifurcate to quadrupled tori which exist in the region denoted by $4T$. On the other hand, chaotic oscillating states with positive largest Lyapunov exponents ($\sigma_1 > 0$) exist in the region shown in black. Between these regular and chaotic regions, SN oscillating states that have negative largest Lyapunov exponents ($\sigma_1 < 0$) and positive phase sensitivity exponents ($\delta > 0$) exist in the region shown in gray. Due to their high phase sensitivity, SN oscillating states have a strange fractal phase space structure leading to aperiodic complex spikings. These SN states are robust ones because they appear in a finite range of the parameter space.[15] Diverse dynamical routes to SN oscillations will be discussed below.

SN attractors appear via gradual fractalization when passing a heavy solid boundary curve in Fig. 2.[8] As an example, we study such transition to SN oscillations along the route a by decreasing A_1 for $A_2 = 1.1$ μA/cm^2. The time series of $V(t)$ for the quasiperiodic oscillation, the SN oscillation, and the chaotic oscillation for $A_1 = 70.9$, 70.67, and 70.5 μA/cm^2 are shown in Figs. 3(a)–(c), respectively. These regular, SN, and chaotic states are analyzed in terms of the largest Lyapunov exponent σ_1 and the phase sensitivity exponent δ in the Poincaré map. Figures 3(d)-(f) show projections of their corresponding attractors onto the θ-V plane. For the regular state, a smooth torus exists in the θ-V plane, as shown in Fig. 3(d). As A_1 is decreased, the smooth torus becomes more and more wrinkled and transforms to an SN attractor without apparent mediation of any nearby unstable invariant set[5),6)] [e.g., see Fig. 3(e)]. This kind of gradual fractaliczation is the most common route to SN attractors. As A_1 is further decreased, such an SN attractor transforms to a chaotic attractor, as shown in Fig. 3(f).

Dynamical property of an attractor is characterized in terms of the largest Lyapunov exponent σ_1. The Lyapunov-exponent diagram (i.e., plot of σ_1 vs A_1) is shown in Fig. 3(g). As A_1 passes a threshold value of $A_1 \simeq 70.729$ μA/cm^2, an SN attractor appears. The graph of σ_1 for the SN attractor is shown in black, and its value is negative like the case of smooth torus. However, when passing the chaotic transition point of $A_1 \simeq 70.621$ μA/cm^2, a chaotic attractor with a positive σ_1 appears. Although SN and chaotic attractors are dynamically different, both of them have strange geometry. For characterizing the strangeness of an attractor, we investigate the sensitivity of the attractor with respect to the phase θ of the external quasiperiodic forcing.[10] This phase sensitivity may be characterized by differentiating $\boldsymbol{x}$ with respect to θ of the quasiperiodic forcing at a discrete time $t = n$. Using Eq. (2·3c), we obtain the following governing equation for $\frac{\partial x_i}{\partial \theta}$ $(i = 1, 2)$,

$$\frac{d}{dt}\left(\frac{\partial x_i}{\partial \theta}\right) = \sum_{j=1}^{2} \frac{\partial F_i}{\partial x_j} \cdot \frac{\partial x_j}{\partial \theta} + \frac{\partial F_i}{\partial \theta}, \tag{2·4}$$

where $(x_1, x_2) = (V, w)$ and F_i $(i = 1, 2)$ are given in Eq. (2·3c). Starting from an initial point $\boldsymbol{x}(0)$ and an initial value $\partial \boldsymbol{x}/\partial\theta = \boldsymbol{0}$ for $t = 0$, we obtain the deriva-

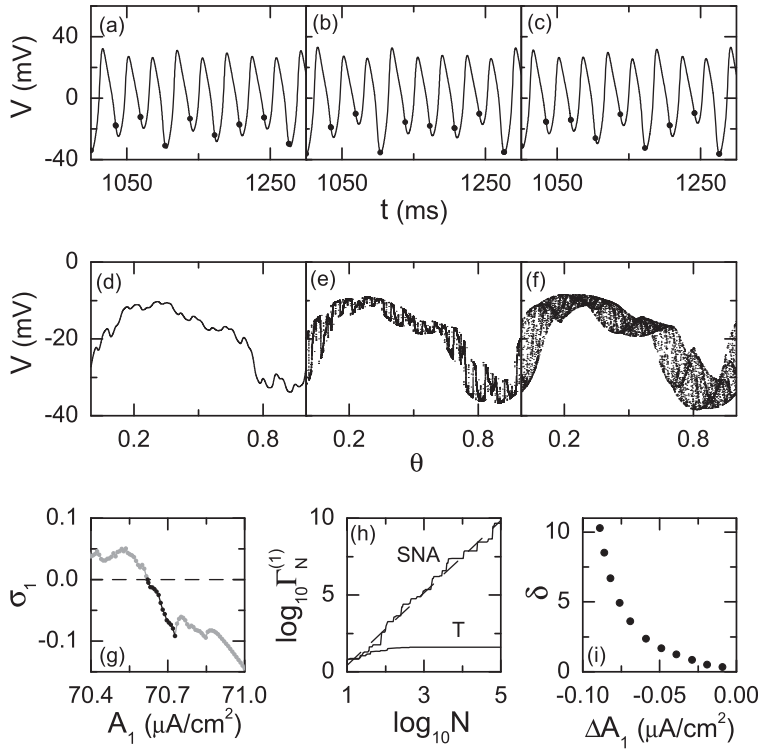

Fig. 3. Appearance of an SN attractor via gradual fractalization along the route a in Fig. 2 for $A_2 = 1.1$ μA/cm^2. Time series of $V(t)$ for (a) the quasiperiodic spiking state ($A_1 = 70.9$ μA/cm^2), (b) the SN spiking state ($A_1 = 70.67$ μA/cm^2), and (c) the chaotic spiking state ($A_1 = 70.5$ μA/cm^2). Solid circles represent stroboscopically sampled points in the Poincaré map P. Projections of attractors onto the θ-V plane in P are shown for (d) the smooth torus [corresponding to (a)], (e) the SN attractor (corresponding to (b)], and (f) the chaotic attractor [corresponding to (c)]. (g) Lyapunov-exponent diagram (i.e., plot of σ_1 vs A_1); σ_1 for the SN attractor is shown in black. (h) Phase sensitivity functions $\Gamma_N^{(1)}$ are shown for the smooth torus (T) [(d)] and the SN attractor (SNA) [(e)]. For the case of the SN attractor, the graph is well fitted with a dashed straight line with slope $\delta \simeq 2.36$. (i) Plot of the phase sensitivity exponent δ versus ΔA_1 ($= A_1 - A_1^*$) for the SN attractor; $A_1^* \simeq 70.729$.

tive values of $S_n^{(i)}$ ($\equiv \partial x_i/\partial\theta$) at all subsequent discrete time $t = n$ by integrating Eqs. (2·3c) and (2·4). One can easily see the boundedness of $S_n^{(i)}$ by looking only at the maximum

$$\gamma_N^{(i)}(\boldsymbol{x}(0)) = \max_{0\le n\le N} |S_n^{(i)}(\boldsymbol{x}(0))| \ . \quad (i = 1, 2) \tag{2·5}$$

Generally, $\gamma_N^{(i)}(\boldsymbol{x}(0))$ depends on a particular trajectory. To obtain a "representative" quantity that is independent of a particular trajectory, we consider an ensemble of randomly chosen initial points $\{\boldsymbol{x}(0)\}$, and take the minimum value of $\gamma_N^{(i)}$ with

respect to the initial orbit points,[10)]

$$\Gamma_N^{(i)} = \min_{\{\boldsymbol{x}(0)\}} \gamma_N^{(i)}(\boldsymbol{x}(0)) \ . \quad (i = 1, 2) \tag{2·6}$$

Figure 3(h) shows a phase sensitivity function $\Gamma_N^{(1)}$, which is obtained in an ensemble containing 20 random initial orbit points $\{(V_i(0), w_i(0));\ i = 1, \ldots, 20\}$ which are chosen with uniform probability in the range of $V_i(0) \in (-20, 20)$, $w_i(0) \in (0.4, 0.5)$, and $\theta_i(0) \in [0, 1)$. For the case of the smooth torus in Fig. 3(d), $\Gamma_N^{(1)}$ grows up to the largest possible value of the derivative $|\partial x_1/\partial\theta|$ along a trajectory and remains for all subsequent time. Thus, $\Gamma_N^{(1)}$ saturates for large N and hence the smooth torus has smooth geometry without phase sensitivity. On the other hand, for the case of the SN attractor in Fig. 3(e), $\Gamma_N^{(1)}$ grows unboundedly with a power δ,

$$\Gamma_N^{(1)} \sim N^{\delta}. \tag{2·7}$$

Here, the value of $\delta \simeq 2.36$ is a quantitative characteristic of the phase sensitivity of the SN attractor, and δ is called the phase sensitivity exponent. For getting satisfactory statistics, we consider 20 ensembles for each A_1, each of which contains 20 randomly chosen initial points and choose the average value of the 20 phase sensitivity exponents obtained in the 20 ensembles. Figure 3(i) shows a plot of δ versus ΔA_1 $(= A_1 - A_1^*)$. We note that the value of δ monotonically increases from zero as A_1 is decreased away from the SN transition point A_1^* $(= 70.729\ \mu\text{A/cm}^2)$. Due to this phase sensitivity, the SN oscillating state has strange fractal geometry leading to aperiodic complex spikings, like the case of chaotic oscillations [e.g., see Figs. 3(b) and (c)].

When passing a dashed boundary curve in Fig. 2, another route to SN attractors appears via collision between a stable smooth doubled torus and its unstable smooth parent torus.[9)] As an example, we study such transition to SN oscillations along the route b by decreasing A_1 for $A_2 = 0.6\ \mu\text{A/cm}^2$. Figure 4(a) shows a stable two-band torus (denoted by a solid curve) and an unstable smooth one-band parent torus (denoted by a short-dashed curve) for $A_1 = 70.44\ \mu\text{A/cm}^2$. We note that the unstable parent torus is located in the middle of the two bands of the stable torus. With decrease in A_1, the bands of the stable torus become more and more wrinkled, while the unstable torus remains smooth [e.g. see Fig. 4(b)]. As A_1 passes a threshold value of $A_1 \simeq 70.4321\ \mu\text{A/cm}^2$, the two bands of the stable torus touch its unstable parent torus at a dense set of θ values (not at all θ values). This phase-dependent (nonsmooth) collision between the stable doubled torus and its unstable parent torus results in the birth of an SN attractor, as shown in Fig. 4(c). This SN attractor, containing the former bands of the torus as well as the unstable parent torus, has a positive phase sensitivity exponent (i.e., $\delta > 0$). We discuss the distribution of local (M-time) Lyapunov exponents σ_1^M, causing the phase sensitivity of the SN attractor.[10)] By taking a long trajectory and dividing it into segments of length M, we calculate σ_1^M for each segment and obtain the probability distribution $P(\sigma_1^M)$. For $M = 100$, 300, and 500, $P(\sigma_1^M)$ are shown in Fig. 4(d). In the limit of $M \to \infty$, $P(\sigma_1^M)$ approaches the delta distribution $\delta(\sigma_1^M - \sigma_1)$, where $\sigma_1 (\simeq -0.019)$ is the

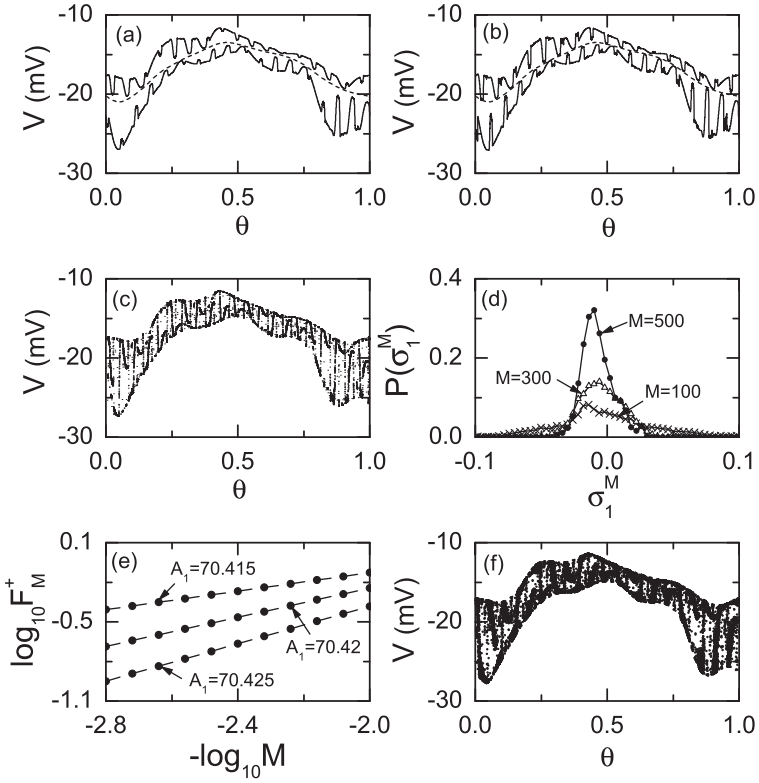

Fig. 4. Appearance of an SN attractor via phase-dependent (nonsmooth) collision between a stable two-band torus and its unstable smooth parent torus along the route b in Fig. 2 for $A_2 = 0.6$ μA/cm^2. Stable two-band torus (denoted by a solid curve) and its unstable smooth torus (represented by a short-dashed curve) for (a) $A_1 = 70.44$ μA/cm^2 and (b) $A_1 = 70.434$ μA/cm^2. (c) SN attractor with $\sigma_1 \simeq -0.019$ and $\delta \simeq 1.81$ for $A_1 = 70.42$ μA/cm^2. (d) Three probability distributions $P(\sigma_1^M)$ of the local M-time Lyapunov exponent for $M = 100$ (circles), 300 (triangles), and 500 (crosses) when $A_1 = 70.42$ μA/cm^2. (e) Three plots of $\log_{10} F_M^+$ versus $-\log_{10} M$ for $A_1 = 70.415$, 70.42, and 70.425 μA/cm^2. (f) Chaotic attractor with $\sigma_1 \simeq 0.012$ for $A_1 = 70.4$ μA/cm^2.

usual averaged Lyapunov exponent. However, we note that the distribution $P(\sigma_1^M)$ has a significant positive tail which does not vanish even for large M. This positive tail results from the local expansion near the embedded unstable parent torus.[5] To quantify this slow decay of the positive tail, we define the fraction of positive local Lyapunov exponents as

$$F_M^+ = \int_0^\infty P(\sigma_1^M)\, d\sigma_1^M. \tag{2·8}$$

These fractions F_M^+ are plotted for $A_1 = 70.415$, 70.42, and 70.425 μA/cm^2 in Fig. 4(e). Note that for each value of A_1, the fraction F_M^+ exhibits a power-law

decay,

$$F_M^+ \sim M^{-\eta}. \tag{2·9}$$

Here, the value of η decreases as A_1 is decreased. Consequently, a trajectory on any SN attractor has segments of arbitrarily long length M that have positive local Lyapunov exponents, and thus it has a phase sensitivity, inducing the strangeness of the SN attractor. As shown in Fig. 4(e), as A_1 is decreased the value of F_M^+ becomes larger. Hence, the degree of phase sensitivity of the SN attractor increases. However, its dynamics is nonchaotic because the averaged Lyapunov exponent is negative (i.e., $\sigma_1 < 0$). As another threshold value of $A_1 \simeq 70.412\ \mu\text{A/cm}^2$ is passed, the SN attractor turns into a chaotic attractor with a positive largest Lyapunov exponent σ_1, as shown in Fig. 4(f).

A main interesting feature of the state diagram in Fig. 2 is the existence of "tongues" of quasiperiodic motion that penetrate into the chaotic region. The first-order (second-order) tongue lies near the terminal point (denoted by a cross) of the first-order (second-order) torus-doubling bifurcation curve. When crossing the upper boundary of the tongue (denoted by a dotted line), an SN attractor exhibiting intermittency appears. This intermittent transition was found to occur via phase-dependent collision of a stable torus with a nonsmooth ring-shaped unstable set in the quasiperiodically forced logistic map.[12),13)] Here, we study the transition to an intermittent SN attractor along the route c in the first-order tongue by increasing A_2 for $A_1 = 70.2\ \mu\text{A/cm}^2$. Figure 5(a) shows a smooth torus for $A_2 = 0.94\ \mu\text{A/cm}^2$. When passing a threshold value of $A_2 \simeq 0.945\,49\ \mu\text{A/cm}^2$, a sudden transition to an intermittent SN attractor occurs, as shown in Fig. 5(b) for $A_2 = 0.9455\ \mu\text{A/cm}^2$. A typical trajectory on the intermittent SN attractor spends a long stretch of time in the vicinity of the former torus, then it bursts out from this region and traces out a much larger fraction of the state space, and so on. To characterize the intermittent bursting, we use a small quantity d^* for the threshold value of the magnitude of the deviation from the former torus. When the deviation is smaller (larger) than d^*, the intermittent attractor is in the laminar (bursting) phase. For each A_2, we follow a long trajectory until 10^4 laminar phases are obtained in the Poincaré map P and get the average of characteristic time τ between bursts. As shown in Fig. 5(c), the average value of τ exhibits a power-law scaling behavior,

$$\overline{\tau} \sim \Delta A_2^{-\gamma}, \quad \gamma \simeq 0.5, \tag{2·10}$$

where the overbar represents time averaging and $\Delta A_2^* = A_2 - A_2^*$ ($A_2^* = 0.94549$). The scaling exponent γ seems to be the same as that for the case of the quasiperiodically forced map.[11)] This SN attractor has a positive phase sensitivity with $\delta \simeq 4.76$ due to the existence of positive local Lyapunov exponents. Figure 5(d) shows the probability distributions of local (M-time) Lyapunov exponents $P(\sigma_1^M)$ for $M = 100,\ 300$, and 500. We note that the distribution $P(\sigma_1^M)$ has a significant positive tail which does not vanish even for large M. This positive tail results from the local expansion near the embedded unstable set.[5)] We quantify this slow decay of the positive tail in terms of the fraction of positive local Lyapunov exponents F_M^+ defined in Eq. (2·8). Such fractions F_M^+ are plotted for $A_1 = 0.94549, 0.9455,$

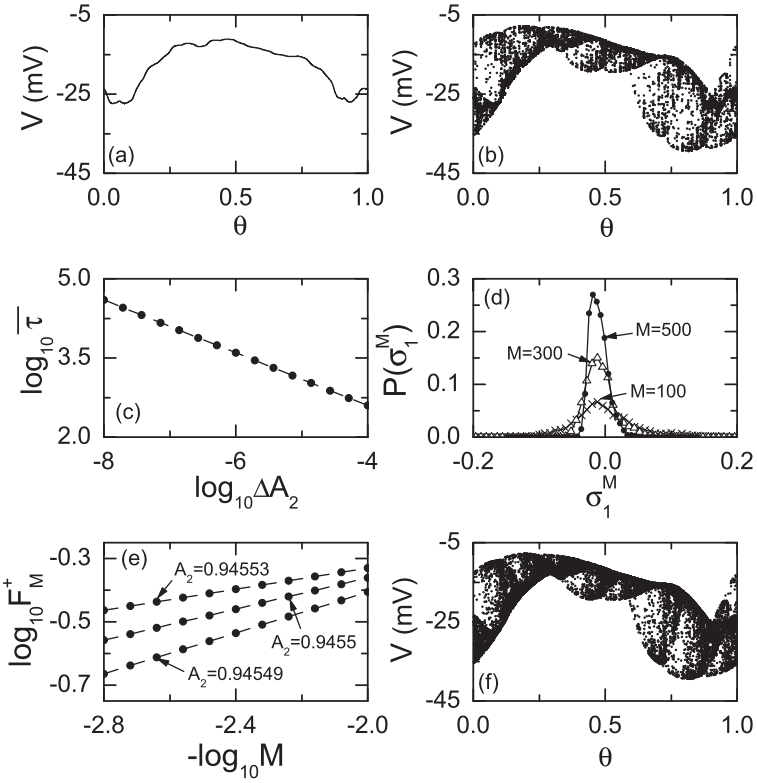

Fig. 5. Appearance of an intermittent SN attractor along the route c in Fig. 2 for $A_1 = 70.2$ μA/cm^2. (a) Smooth torus with $\sigma_1 \simeq -0.125$ for $A_2 = 0.94$ μA/cm^2. (b) Intermittent SN attractor with $\sigma_1 \simeq= -0.012$ and $\delta \simeq 4.76$ for $A_2 = 0.9455$ μA/cm^2. (c) Plot of $\log_{10}\overline{\tau}$ vs $\log_{10}\Delta A_2$. The graph is well fitted with a dashed straight line with slope $\gamma \simeq 0.5$. Here $\overline{\tau}$ is the average characteristic time between bursts and $\Delta A_2 = A_2 - A_2^*$ ($A_2^* = 0.94549$ μA/cm^2). For each ΔA_2, $\overline{\tau}$ is calculated from 10^4 laminar phases in the Poincaré map P. (d) Three probability distributions $P(\sigma_1^M)$ of the local M-time Lyapunov exponent for $M = 100$ (circles), 300 (triangles), and 500 (crosses) when $A_2 = 0.9455$ μA/cm^2. (e) Three plots of $\log_{10} F_M^+$ versus $-\log_{10} M$ for $A_2 = 0.94549, 0.9455$, and 0.94553 μA/cm^2. (f) Chaotic attractor with $\sigma_1 \simeq 0.038$ for $A_2 = 0.948$ μA/cm^2.

and 0.94553 μA/cm^2 in Fig. 5(e). Note that for each value of A_2, the fraction F_M^+ exhibits a power-law decay, $F_M^+ \sim M^{-\eta}$, where the value of η decreases as A_2 is increased. As a result, a trajectory on any SN attractor has segments of arbitrarily long length M that have positive local Lyapunov exponents, and thus it has a phase sensitivity, inducing the strangeness of the SN attractor. However, its dynamics is nonchaotic because the averaged Lyapunov exponent is negative (i.e. $\sigma_1 < 0$) in the limit of $M \to \infty$. As another threshold value of $A_2 \simeq 0.9456$ μA/cm^2 is passed, the SN attractor transforms to a chaotic attractor with a positive largest Lyapunov exponent σ_1 [see Fig. 5(f)]. As in this case of the first-order tongue, similar transition

from a smooth doubled torus to a single-band intermittent SN attractor also occurs when passing the upper dotted boundary curve of the second-order tongue.

§3. Summary

We have studied dynamical responses of the self-oscillating ML neuron under quasiperiodic stimulation andquasiperiodic stimulation and compared them with those for the case of periodic stimulus. In the periodically-forced case, a transition from a periodic to a chaotic oscillation has been found to occur through period doublings. We have investigated the effect of the quasiperiodic forcing on the period-doubling route to chaotic oscillation. Unlike the case of periodic forcing, a new type of SN oscillating states has been found to appear between the regular and chaotic oscillating states. Strange geometry of the SN attractors, which is characterized in terms of the phase sensitivity and the distribution of local finite-time Lyapunov exponent, leads to aperiodic complex spikings. Diverse routes to SN oscillations have been found, as in the quasiperiodically forced logistic map. These SN attractors are also found to appear in both the Hodgkin-Huxley neuron and the FitzHugh-Nagumo neuron under quasiperiodic forcing.[23] Hence, the dynamical routes to SN states seem to be "universal" because they occur in typical quasiperiodically forced period-doubling systems of different nature. Finally, we suggest a real experiment on the quasiperiodically forced neuron (e.g., a squid giant axon) and expect SN dynamical responses to be observed.

Acknowledgements

This work was finalized while S.-Y. Kim was spending his sabbatical year (supported by the Kangwon National University) in the University of Wisconsin-Milwaukee. S.-Y. Kim thanks Prof. Yakovlev for hospitality.

References

1) M. R. Guevara, L. Glass and A. Shrier, Science **214** (1981), 1350.
L. Glass, M. R. Guevara, A. Shrier and R. Perez, Physica D **7** (1983), 89.
2) K. Aihara, T. Numajiri, G. Matsumoto and M. Kotani, Phys. Lett. A **116** (1986), 313.
N. Takahashi, Y. Hanyu, T. Musha, R. Kubo and G. Matsumoto, Physica D **43** (1990), 318.
D. T. Kaplan, J. R. Clay, T. Manning, L. Glass, M. R. Guevara and A. Shrier, Phys. Rev. Lett. **76** (1996), 4074.
3) L. Glass and M. C. Mackey, *From Clocks to Chaos* (Princeton University Press, Princeton, 1988).
4) M. Ding and J. A. S. Kelso, Int. J. Bifurction Chaos Appl. Sci. Eng. **2** (1992), 295.
5) U. Feudel, S. Kuznetsov and A. Pikovsky, *Strange Nonchaotic Attractors* (World Scientific, Singapore, 2006).
6) A. Prasad, S. S. Negi and R. Ramaswamy, Int. J. Bifurcation Chaos Appl. Sci. Eng. **11** (2001), 291.
7) C. Grebogi, E. Ott, S. Pelikan and J. A. Yorke, Physica D **13** (1984), 261.
8) K. Kaneko, Prog. Theor. Phys. **72** (1984), 202.
T. Nishikawa and K. Kaneko, Phys. Rev. E **54** (1996), 6114.
9) J. F. Heagy and S. M. Hammel, Physica D **70** (1994), 140.
10) A. S. Pikovsky and U. Feudel, Chaos **5** (1995), 253.

11) A. Prasad, V. Mehra and R. Ramaswamy, Phys. Rev. Lett. **79** (1997), 4127.
12) S.-Y. Kim, W. Lim and E. Ott, Phys. Rev. E **67** (2003), 056203.
S.-Y. Kim and W. Lim, J. of Phys. A **37** (2004), 6477.
13) W. Lim and S.-Y. Kim, Phys. Lett. A **335** (2005), 383.
14) W. Lim and S.-Y. Kim, Phys. Lett. A **355** (2006), 331.
S.-Y. Kim and W. Lim, Phys. Lett. A **334** (2005), 160.
15) J.-W. Kim, S.-Y. Kim, B. Hunt and E. Ott, Phys. Rev. E **67** (2003), 036211.
16) W. L. Ditto, M. L. Spano, H. T. Savage, S. N. Rauseo, J. Heagy and E. Ott, Phys. Rev. Lett. **65** (1990), 533.
W. X. Ding, H. Deutsch, A. Dinklage and C. Wilke, Phys. Rev. E **55** (1997), 3769.
B. P. Bezruchko, A. P. Kuznetsov, and Y. P. Seleznev, Phys. Rev. E **62** (2000), 7828.
K. Thamilmaran, D. V. Senthikumar, A. Venkatesan and M. Lakshmanan, Phys. Rev. E **74** (2006), 036205.
17) C. Morris and H. Lecar, Biophys. J. **35** (1981), 193.
18) J. Rinzel and B. Ermentrout, in *Methods in Neural Modeling: from Ions to Networks*, ed. C. Koch and I. Segev (MIT Press, Cambridge, 1998), p. 251.
19) K. Tsumoto, H. Kitajima, T. Yoshinaga, K. Aihara and H. Kawakami, Neurocomputing **69** (2006), 293.
20) K. Aihara, G. Matsumoto and Y. Ikegaya, J. Theor. Biol. **109** (1984), 249.
K. Aihara, T. Numajiri, G. Matsumoto and M. Kotani, Phys. Lett. A **116** (1986), 313.
N. Takahashi, Y. Hanyu, T. Musha, R. Kubo and G. Matsumoto, Physica D **43** (1990), 318.
D. T. Kaplan, J. R. Clay, T. Manning, L. Glass, M. R. Guevara and A. Shrier, Phys. Rev. Lett. **76** (1996), 4074.
21) M. J. Feigenbaum, J. Stat. Phys. **21** (1979), 669.
22) A. J. Lichtenberg and M. A. Lieberman, *Regular and Stochastic Motion* (Springer-Verlag, New York, 1983), p. 283.
23) W. Lim and S.-Y. Kim, unpublished.